

---

# Classical State Preparation for Variational Quantum Algorithms via Reinforcement Learning

---

Gino Kwun

Dhanvi Bharadwaj

Gokul Subramanian Ravi

Computer Science and Engineering  
 University of Michigan  
 Ann Arbor, MI 48109, USA  
 {gkwun, dhanvib, gsravi}@umich.edu

## Abstract

Variational Quantum Algorithms (VQAs) potentially offer a pathway to practical quantum advantage, but their optimization is heavily hindered by barren plateaus and numerous local minima. While classically simulable Clifford circuits can warm-start VQAs to accelerate convergence, existing heuristic-based initialization methods struggle to scale within vast combinatorial search spaces. To overcome this bottleneck, we propose CRiSP (a Clifford Reinforcement Learning agent for State Preparation), a framework that formulates discrete prefix selection as a sequential decision-making problem. CRiSP utilizes Neural-Guided Monte Carlo Tree Search, driven by a Transformer-based policy trained via self-play, to insert learned Clifford gates before fixed parameterized rotations. This enables the construction of high-quality initial states entirely through polynomial-time classical stabilizer simulation without altering the underlying circuit architecture. By integrating a curriculum learning strategy that progressively expands the search horizon, the agent efficiently scales to deep circuits. Evaluated on QAOA benchmarks of up to 22 qubits and 1,370 parameters, CRiSP outperforms state-of-the-art Clifford initialization methods by a mean of  $3.17\times$  (max  $45.02\times$ ) in average energy accuracy and  $2.44\times$  (max  $16.01\times$ ) in best-achieved energy accuracy. Assessments on VQE tasks further demonstrate the framework’s robustness and generalizability.

## 1 Introduction

The potential for quantum computing to deliver a computational edge is particularly strong in domains such as chemistry [47], optimization [66], and machine learning [7]. The field is currently evolving past the era of Noisy Intermediate-Scale Quantum (NISQ) hardware [74], approaching a transition phase characterized by devices with thousands of physical qubits, augmented by advanced error mitigation and early forms of quantum error correction [45, 30, 44, 48]. While executing deeply complex routines like Shor’s or Grover’s algorithms [89, 34] remains out of reach due to strict fault-tolerance requirements [69], Variational Quantum Algorithms (VQAs) [14] possess an inherent resilience to hardware noise. Operating as hybrid quantum-classical frameworks, VQAs employ a classical optimizer to iteratively update a parameterized quantum circuit, navigating the solution landscape to minimize a target energy expectation value ( $\langle H_c \rangle$ ) [72, 49, 22]. Consequently, working toward the enhancement and optimization of VQA execution on early fault-tolerant quantum hardware is of critical importance today.

As the field advances toward the fault-tolerant era, the practical cost of each VQA iteration becomes heavily bottlenecked by the execution of non-Clifford gates, which demand immense overhead [53]. Given this per-iteration resource cost, it is critical to limit the total number of VQA evaluations. However, VQA optimization landscapes are notoriously difficult to navigate, frequently forcing optimizers to evaluate thousands of expensive circuits just to make marginal progress. To

bypass these optimization traps and drastically reduce required circuit executions, there is a strong motivation for developing classically tractable state preparation and initialization strategies [78, 86, 6]. Among simulation-compatible gate sets, the Clifford group provides a theoretically principled discrete search space. Since Clifford circuits can be simulated in polynomial time classically, they enable exact computation of the initial energy expectation value without requiring quantum hardware. Existing Clifford initialization methods exploit this simulability through Bayesian or genetic-algorithm-based heuristics [78, 6]. However, when confronted with challenging optimization landscapes, these naive discrete search techniques often struggle to navigate the vast combinatorial space. An overview of VQA and classical state preparation to initialize it is shown in Fig. 1.

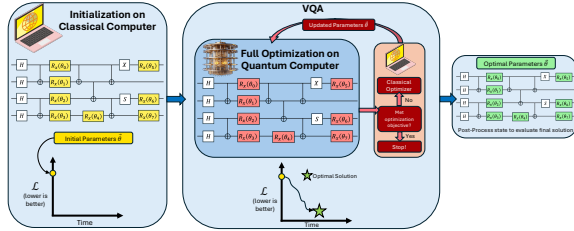


Figure 1: Classical initialization for VQA.

To overcome the scaling limitations of standard heuristics, we formulate discrete initialization as a sequential decision-making problem suited for reinforcement learning (RL) [94]. Specifically, we take an ansatz with fixed rotational gate positions and prepend a discrete Clifford gate to each rotation to act as a prefix modifier. When all continuous parameters are initialized to  $\theta = 0$ , the rotation gates reduce to the identity up to a global phase, meaning the resulting circuit state is determined entirely by the chosen Clifford prefix configuration. This casts the initialization problem as a combinatorial search task—a domain where RL consistently demonstrates strong performance [24, 63]—all without altering the original parameterized structure.

We present a Clifford Reinforcement Learning agent for State Preparation (CRiSP), a discrete-gate warm-start framework for VQAs. Utilizing Neural-Guided Monte Carlo Tree Search (NG-MCTS) [90], the agent navigates the discrete Clifford space via classical simulation, selecting sequential Clifford gates that minimize the Hamiltonian expectation value. Further, for tasks with large parameter counts and sparse energy signals, we introduce an incremental horizon curriculum that gradually expands the search horizon during training. At each decision step, the search is driven by a Transformer-based [97] policy and value network, which encodes the current gate sequence to output prior probabilities for the next gate alongside an estimated return. The episodic reward is defined as the negative expectation energy of the synthesized circuit, and the agent leverages two types of replay buffers [24, 90] to enhance training efficiency.

While CRiSP is broadly applicable to any VQA, we primarily focus on its benefits for the Quantum Approximate Optimization Algorithm (QAOA) [22], benchmarking against the SPIQ [6] initialization framework on combinatorial optimization problems including MaxCut, Knapsack, and feature selection using high-order medical datasets. We also provide an auxiliary evaluation for the Variational Quantum Eigensolver (VQE) [72] to illustrate the generalizability of our approach.

Overall, this work makes three primary contributions. First, we formalize Clifford prefix initialization in VQA as a sequential decision-making problem over the discrete gate space, developing an RL framework that is classically simulable and avoids exponential state representations. Second, we introduce CRiSP, a Transformer-guided tree search agent trained via self-play over the Clifford prefix space, incorporating a curriculum [5] with a stepwise increase in episode length to handle long-horizon tasks. Third, we empirically evaluate on QAOA benchmarks across systems of up to 22 qubits and 1,370 circuit parameters, demonstrating that CRiSP consistently outperforms the current state-of-the-art in initialization by a mean of  $3.17\times$  (max  $45.02\times$ ) in average energy accuracy and  $2.44\times$  (max  $16.01\times$ ) in best achieved energy accuracy, given the same evaluation budget.

## 2 Background and related work

**Variational quantum algorithms and optimization traps.** VQAs are iterative hybrid quantum-classical methods, including the VQE [72] and the QAOA [22]. VQE is widely used in quantum chemistry and condensed matter physics, whereas QAOA targets combinatorial optimization problems, particularly Quadratic Unconstrained Binary Optimization (QUBO). In each VQA iteration, a classical optimizer [54, 92] updates a parameterized quantum circuit (ansatz) to approximate the ground-state

energy of a problem Hamiltonian [64]. However, achieving rapid convergence is notoriously difficult. VQA optimization landscapes feature numerous local minima and barren plateaus [65, 83, 8]—regions where gradients vanish exponentially as circuit size and depth increase. These traps make convergence from arbitrary initial points highly unreliable, potentially curtailing quantum benefits.

**Fault-tolerant costs and classical simulatability.** With the emergence of Fault-Tolerant Quantum Computing (FTQC) execution [88], hardware-efficient circuit synthesis is a central issue [47]. The practical cost of each VQA iteration is governed heavily by the count of non-Clifford gates [53]. Non-Clifford rotation gates, such as  $R_x$  and  $R_z$ , must be approximately decomposed into a universal gate set supported by the underlying hardware, most commonly the Clifford+ $T$  set, using compilers such as Gridsynth [81] or tensor-network-based synthesizers [37]. Because implementing a single  $T$  gate demands resource-intensive procedures like magic state distillation [12] and cultivation [27], the cumulative overhead of every execution is substantial. Notably, a specific subset of these synthesized sequences corresponds entirely to the Clifford group. By the Gottesman-Knill theorem, any quantum circuit composed exclusively of these Clifford gates can be simulated in polynomial time and space via stabilizer tableau methods [31, 1]. This enables exact computation of the energy expectation value (within the Clifford-only quantum state space) without requiring quantum hardware [26].

**Classical VQA initialization.** VQA performance is highly sensitive to initialization [32]. While early heuristics like INTERP [104], TQA [84], and identity block initialization [32] are often problem-specific, Clifford-based methods leverage stabilizer simulability for broader applicability. For instance, CAFQA [78] and Cheng et al. [15] use Bayesian optimization and simulated annealing, respectively, for Clifford-only initialization. Clapton [86] adds noise-aware transformations and a genetic algorithm, while SPIQ [6] adapts this for QAOA [22]. However, these randomized or population-based heuristics struggle to scale across vast combinatorial spaces. In contrast, our framework learns a search policy to systematically discover high-quality Clifford gate sequences *a priori* for every rotation gate. Embedding these discrete structures into the starting circuit turns continuous parameter optimization and gate synthesis into an incremental refinement over a classically pre-computed configuration, drastically improving efficiency.

**Reinforcement learning for quantum search.** RL [94] shows strong potential in quantum applications, from error correction [91] to circuit optimization [101]. Search-based methods like MCTS [13] and AlphaZero [90] effectively navigate massive combinatorial spaces [24]. Within the quantum domain, AlphaTensor-Quantum [82] applies learned search to minimize T-counts. Most similarly, MCTS-QAOA [102] jointly optimizes discrete and continuous variables, but relies on costly quantum circuit evaluations during search. In contrast, CRiSP formulates prefix selection as a sequential decision-making problem entirely within the classically simulable Clifford space. By training a Transformer-based policy-value network, we enable principled exploration while eliminating the need for quantum hardware overhead during initialization.

### 3 Methods

In this section, we describe the configuration of the reinforcement learning (RL) environment and agent for the VQA state preparation task, as depicted in Figure 2, given a problem Hamiltonian and a fixed underlying circuit structure. We first specify the environment’s state, action, and reward formulations. We then introduce CRiSP, the NG-MCTS agent that performs stepwise inference to identify the Clifford prefix configuration yielding the lowest circuit energy, alongside its self-play training procedure and a curriculum variant. Formally, given an  $n$ -qubit cost Hamiltonian  $H_c$  and a fixed ansatz containing  $D = \text{poly}(n)$  rotational gates, such as hardware-efficient and QAOA architectures [47, 22, 14], we cast the state preparation process as a Markov Decision Process (MDP)  $(\mathcal{S}, \mathcal{A}, \mathcal{T}, \mathcal{R}, \gamma)$ . The agent’s objective is to construct a gate sequence that prepares a quantum state  $|\psi\rangle$  minimizing the expected energy  $E = \langle H_c \rangle = \langle \psi | H_c | \psi \rangle$ .

#### 3.1 RL environment

The **state**  $s_t$  at step  $t$  in the RL environment is defined as the ordered sequence of Clifford gates assigned to the first  $t$  prefix positions, prepended with a special START token. Since the sequence length scales linearly with  $D$ , this representation avoids the exponential dimensionality incurred by storing the raw quantum state vector [67]. Transitions are deterministic, where  $s_{t+1}$  is formed by

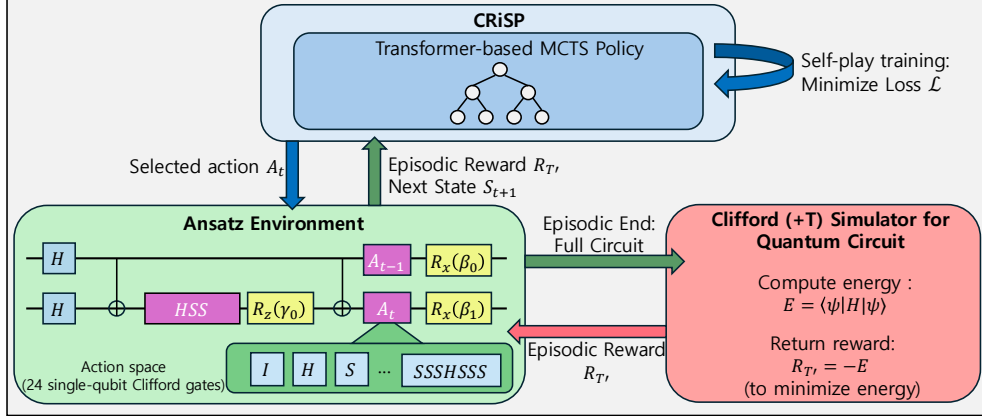


Figure 2: Overview of our proposed neural-guided framework (CRiSP) for state preparation in VQAs. The HSS gate positioned before  $R_z(\gamma_0)$  represents the action  $A_{t-2}$ . The environment depicts a multi-angle QAOA ansatz [41]. The circuit’s final state  $|\psi\rangle$  is generated by setting  $\gamma_0 = \beta_0 = \beta_1 = 0$ .

appending gate action  $a_t$  to  $s_t$ . An episode begins with the state containing only the START token and terminates either when prefixes for all gate positions have been assigned ( $t = D$ ) or when the agent reaches the maximum number of steps  $T'$  ( $t = T'$ ).

The **action space** comprises all 24 single-qubit Clifford gates [21], each representing a candidate prefix modifier for the corresponding rotational gate, since the target gates are single-qubit operations. We consider all axes regardless of the axis of the associated rotation gate, retaining the possibility of identifying configurations that yield favorable energy through interactions with other circuit components. While exhaustive search over the discrete Clifford space of  $24^D$  configurations is intractable for practical system sizes, the proposed RL agent addresses this by concentrating exploration on promising regions, effectively reducing the number of nodes evaluated during tree traversal.

The **reward**  $R$  is provided upon episode termination and is defined as the negative energy expectation value of the synthesized circuit under  $H_c$ ,  $R = -E = -\langle H_c \rangle = -\langle \psi | H_c | \psi \rangle$ , where the resulting state  $|\psi\rangle$  is obtained by setting all continuous parameters to  $\theta = 0$ . Intermediate transitions receive zero reward, and the discount factor is set to  $\gamma = 1$ , reflecting the episodic nature of the task. Since all gates in the synthesis procedure are Clifford, the reward can be evaluated efficiently via a classical stabilizer tableau simulator such as Stim [26]. Because the magnitude of  $\langle H_c \rangle$  varies substantially across different Hamiltonians, ranging from sub-unit values to quantities exceeding  $10^4$ , directly using the raw reward as a training target introduces significant gradient instability. To address this, reward targets are normalized using a running mean  $\mu$  and standard deviation  $\sigma$  as  $R_{\text{norm}} = \frac{R - \max(\mu, 0)}{\sigma + \epsilon} - 1$ , where  $\epsilon$  is a small numerical offset. The  $-1$  term penalizes  $R = 0$  cases, encouraging the agent to seek negative energies (positive rewards). The normalized reward is subsequently clipped to  $[-1, 1]$  to suppress instability from outlier values. This adaptive modification continuously rebalances the reward range throughout training, sustaining active search for higher-return configurations.

### 3.2 The CRiSP framework

We now introduce CRiSP, a Clifford Reinforcement Learning agent for State Preparation in VQA, which utilizes Neural-Guided MCTS (NG-MCTS) to discover the best gate action in each step.

**NG-MCTS procedure.** At each step within an episode, CRiSP selects the next gate action via MCTS guided by a neural network that estimates the expected return of a given state and the prior action probabilities used in simulation [90]. The search proceeds through three stages, namely selection, expansion, and backpropagation. In the **selection** phase, the agent traverses the tree by iteratively choosing actions according to the following upper confidence bound (UCB) criterion [90] when in state  $s$ ,

$$a_{\text{next}} = \arg \max_a \left( Q(s, a) + c_{\text{puct}} \cdot P(s, a) \cdot \frac{\sqrt{N(s)}}{1 + N(s, a)} \right), \quad (1)$$

where  $Q(s, a)$  is the empirical expected state-action value,  $P(s, a)$  is the prior probability predicted by the network, and  $N(s)$  and  $N(s, a)$  denote the visit counts of the parent and child nodes, respectively. The coefficient  $c_{\text{puct}}$  controls the degree of exploration within each simulation, where higher values encourage broader search. To further promote exploration, Dirichlet noise [90] is injected into the root node prior probabilities at the start of each simulation step. Upon reaching a leaf node, the tree undergoes **expansion**, where new child nodes are added and the neural network evaluates the leaf state value along with prior probabilities for its children. If the leaf is a terminal node, no expansion occurs and the estimated value is passed directly to the next procedure. During **backpropagation**, this value is propagated upward to the root, updating the mean state-action values and visit counts of all non-terminal nodes along the traversed path. After collecting  $m$  simulation results per step, the agent samples the next gate proportionally to the visit counts of the child nodes. To balance exploration and exploitation and to facilitate convergence, step-wise decay is applied to the temperature  $\tau$  during the sampling of the next action [90]. Between consecutive steps within an episode, the search tree is reused by re-rooting at the selected action node, improving simulation quality.

**Neural network architecture.** The policy and value networks directing MCTS are composed of four modules: an embedding layer, a shared network, a policy head, and a value head. Given the current gate sequence and the problem Hamiltonian, the embedding layer maps each input token into a dense vector representation augmented with sinusoidal positional encodings [97]. Hamiltonian terms are encoded via one-hot representations of their Pauli structure, with coefficients normalized to balance the relative contribution of each term and prevent numerical instability from outliers. The Hamiltonian encoding is added to the state embedding with a learnable scaling value, forming the input embedding to the shared network. The shared network is a multi-head Transformer encoder [97], which captures sequential dependencies among gate tokens in the current prefix. From the final hidden representation, two separate heads produce distinct outputs, where the policy head applies a softmax over the action space to generate prior probabilities for the next gate and the value head computes a scalar estimate of the expected return. To improve value discrimination among states at the same prefix depth, the value head receives the concatenation of the final Transformer output with the embedding of the most recently added gate token as input. To bound memory consumption, the model processes only the last  $c_{\text{ctx}}$  tokens of the sequence, where  $c_{\text{ctx}}$  is a hyperparameter. Layer normalization [3] and the GELU activation function [40] are employed in the model to stabilize forward-pass signal propagation.

**Agent training.** The neural network is trained through experience replay to progressively improve simulation quality. At each episode step, a sample consisting of the current gate prefix, the MCTS-derived policy target, and the terminal episode reward is stored in a replay buffer. In addition, a compact best-game buffer [24, 90] retains high-and-positive-reward trajectories to facilitate convergence toward promising regions of the search space, as well as to prevent zero or negative signals dominating the learning process. In each training round, the network is trained for  $K$  epochs using the AdamW optimizer [60] and a linear learning rate warmup [97], with each epoch sampling mini-batches from the replay buffer mixed with a fixed proportion of best-game samples once a sufficient number of episodes have been collected. The total training loss  $\mathcal{L}$  combines policy and value objectives as:  $\mathcal{L} = \mathcal{L}_p + c_v \mathcal{L}_v$ , where  $\mathcal{L}_p$  is the cross-entropy loss [61] between the current policy output and the MCTS-derived target distribution and  $\mathcal{L}_v$  is the Huber loss [42] between the predicted and realized returns, balanced by the coefficient  $c_v$ . Throughout training, the policy is periodically evaluated by greedily selecting the highest-probability action at each step with  $m_{\text{eval}}$  MCTS simulations and reduced Dirichlet noise, tracking whether the learned model recovers the high-reward configurations found during training.

### 3.3 Curriculum learning for long-horizon and sparse-reward tasks

To address tasks with extremely large maximum episode lengths and sparse-reward signals by progressively guiding the agent through increasingly complex search horizons, we devise a curriculum variant of CRiSP, which we call the incremental horizon curriculum. Inspired by Bengio et al. [5]

and the role of horizon length in offline RL scalability [70], this strategy consists of three stages with monotonically increasing maximum step counts. This curriculum is made possible by the early-termination property of the target RL environment, which enables the episodic evaluation at any circuit construction step by treating all unassigned prefix positions as identity ( $I$ ) gates. Specifically, the agent operates with 25% of the full episode length ( $0.25T'$ ) until 25% of total training episodes have elapsed, then expands to 50% ( $0.5T'$ ) until the midpoint of training, and finally opens the complete horizon ( $T'$ ) for the remainder. Although this naive staged schedule may be suboptimal for some cases, empirical results confirm that the strategy is particularly effective on benchmarks with large search spaces and limited simulation budgets, where concentrating early training on shorter, tractable sequences accelerates identification of promising partial configurations.

## 4 Evaluation

In this section, we evaluate CRiSP on multiple standard VQA benchmarks of practical interest. We first detail the experimental methodology (Sec. 4.1) and present the QAOA benchmark results (Sec. 4.2). Next, we conduct ablation studies to investigate the impact of the incremental horizon curriculum on large-scale problems and sparse reward environments (Sec. 4.3). Finally, we present exploratory results applying CRiSP to the VQE domain to demonstrate the broader generalizability of our approach (Sec. 4.4).

### 4.1 Methodology

**QAOA benchmarks.** To evaluate CRiSP, we consider three classes of combinatorial optimization problems, with Hamiltonian derivations following [6]. First, we adopt MaxCut on weighted complete graphs as our primary Quadratic Unconstrained Binary Optimization (QUBO) benchmark, providing highly entangled and globally coupled optimization landscapes. Second, for Polynomial Constrained Binary Optimization (PCBO) evaluation, we utilize the Knapsack problem formulated as a Polynomial Unconstrained Binary Optimization (PUBO) Hamiltonian [75]. Third, we evaluate a biomedical high-order feature selection task [87], comprising the “MedicalDense” and “MedicalSparse” benchmarks. We specifically include the latter because its extreme sparsity induces severe barren plateaus, presenting a critical challenge for VQA optimization. Detailed mathematical formulations for these Hamiltonians are deferred to Appendix C.4.

**Comparative baseline.** To benchmark the quality of the classically-prepared state for these QAOA tasks, we compare CRiSP against SPIQ [6], a state-of-the-art Clifford initialization method leveraging a genetic algorithm (GA). All QAOA experiments are conducted in multi-angle QAOA [41] circuits with  $p = 1$ , where all parameterized rotations are relaxed, thereby allowing each parameter to have its respective gate prefix.

**Metrics.** To enable consistent performance comparison across all tasks with substantially different energy scales, we report an accuracy metric similar to that employed in [6], defined as  $\text{Accuracy} = E_{\text{best}}/E_{\text{opt}}$ , where  $E_{\text{best}}$  denotes the minimum energy achieved by a given method and  $E_{\text{opt}}$  is the ground-state energy of the corresponding Hamiltonian. Across experiments, we employ three random seeds and report the mean and standard deviation of the results.

**Implementation details.** MCTS trajectory collection is distributed across 30 parallel workers, forming 30 episodes per training round. The training mini-batch size is set to 512 or 1024 depending on the problem size. We employ a two-stage simulation schedule, in which the agent begins with  $m = 50$  simulations per step during the warmup period, which is the first 10% of the total episodes, to allow rapid exploration, then transitions to a standard phase with  $m = 100$  simulations to enhance search quality. The evaluation simulation count  $m_{\text{eval}}$  is set equal to that of the standard phase. The model is trained using AdamW [60] with a peak learning rate of  $10^{-4}$  and a linear learning rate warmup [97] during the initial stage with a reduced simulation count. To facilitate convergence, a step-wise exponential temperature decay [90] is applied to  $\tau$  after the warmup episodes, starting from  $\tau = 1.0$  at step 25 until a horizon-dependent threshold is met, after which  $\tau$  is held at 0.75. When the incremental horizon curriculum is applied, we use reduced  $c_{\text{puct}}$  to enhance convergence on large tasks, while a grid search over  $c_{\text{puct}} \in \{1, 1.5\}$  is performed in sparse-reward environments. To encourage exploration upon each horizon expansion, the temperature is temporarily set to  $\tau = 1.2$  for

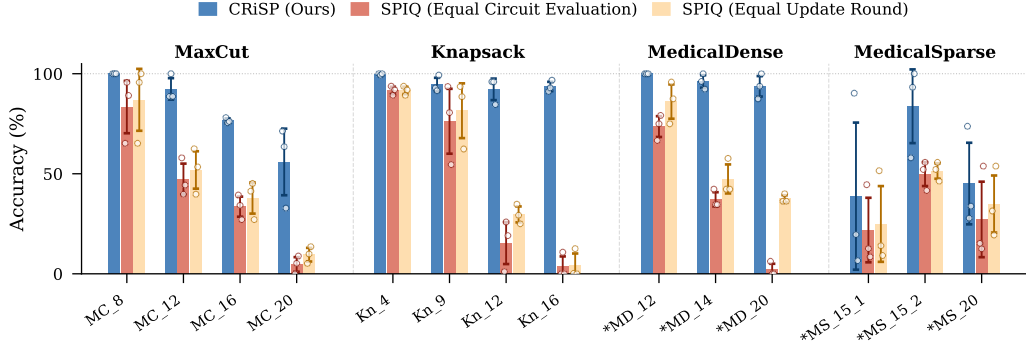


Figure 3: Classical initialization accuracy for QAOA benchmarks. Asterisks (\*) indicate tasks using the incremental horizon curriculum. The bar reflects the average accuracy, the error bar represents the standard deviation (std), and the points show results from three independent runs.

the subsequent 5% of episodes, applied only to gate selection steps within the newly expanded portion of the search horizon. Depending on the problem size, hyperparameters including simulation counts, training episodes, epochs, and learning rates are adjusted based on resource constraints. Further details are provided in Appendix A.

## 4.2 QAOA results

To assess the effectiveness of CRiSP, we compare the proposed agent against SPIQ [6] on a suite of combinatorial optimization problems formulated as Hamiltonians. These include MaxCut on weighted complete graphs, the Knapsack problem, and a biomedical high-order interaction task [87]. Both methods employ QAOA circuit architectures to search for the ground state of each respective Hamiltonian. While CRiSP is broadly applicable to arbitrary Parameterized Quantum Circuits (PQCs), we adopt a multi-angle QAOA [41] framework with a single repetition ( $p = 1$ ) to ensure a fair comparison, as the SPIQ baseline is specifically tailored to such architectures. Following [6], we set the population size of each GA generation to 100. However, we adopt a single-start configuration, as our empirical testing showed that it generally yields superior performance to the original multi-start setting under an equivalent computational budget.

Since both frameworks rely on iterative refinement processes to improve solutions using accumulated performance data, we evaluate SPIQ under two comparative conditions. Our primary baseline matches SPIQ to CRiSP by the total number of circuit evaluations. However, as a supplementary baseline, we also report SPIQ performance matched by the number of update iterations (where SPIQ generations are equated to CRiSP’s training rounds, with each CRiSP round comprising episode collection from 30 workers followed by  $K$  epochs of network updates). Furthermore, for the medical benchmarks [87]—which either feature extreme episode lengths reaching up to 1,370 parameters (referred to as MedicalDense) or exceptionally sparse reward landscapes (MedicalSparse)—we report CRiSP results utilizing the incremental horizon curriculum detailed in Section 3.3.

Figure 3 summarizes the QAOA benchmark results, demonstrating that CRiSP consistently achieves higher energy accuracy than the competing approaches across all tasks (see Appendix B for numerical details). With an overall mean accuracy of 83.03% across 14 distinct tasks, CRiSP outperforms the evaluation-matched SPIQ baseline by a geometric mean (GeoMean) of  $3.17\times$  in average energy accuracy and  $2.44\times$  in best-achieved energy accuracy. Maximum improvements peak at  $45.02\times$  and  $16.01\times$ , respectively, on the MedicalDense\_20 task. When matched by update rounds instead of evaluations, CRiSP continues to surpass SPIQ, achieving GeoMean improvements of  $2.5\times$  (average) and  $2.15\times$  (best), with maximum gains of  $22.51\times$  (average) and  $16.01\times$  (best), again on the MedicalDense\_20 benchmark.

A categorical breakdown further underscores the robustness of the proposed framework. Compared to the evaluation-matched baseline, CRiSP achieves GeoMean improvements of  $2.83\times$  (average) and  $2.32\times$  (best) on MaxCut,  $3.81\times$  (average) and  $2.48\times$  (best) on Knapsack, and  $5.41\times$  (av-

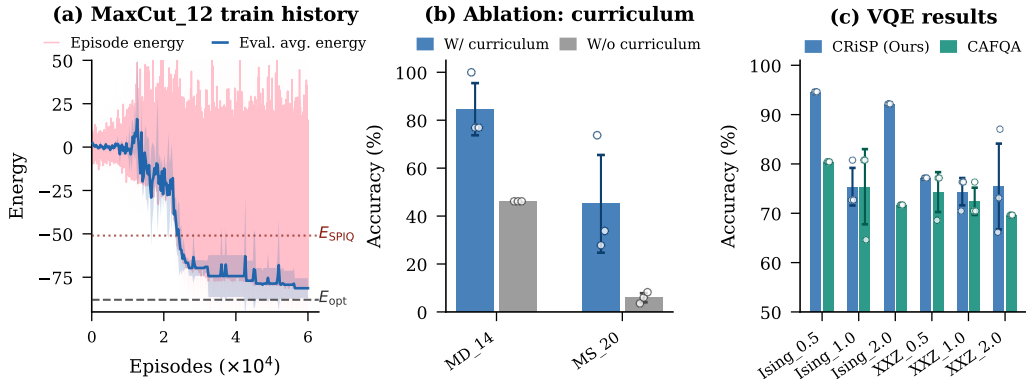


Figure 4: (a) Training history of MaxCut\_12 benchmark.  $E_{\text{opt}}$  and  $E_{\text{SPIQ}}$  denote the ground-state and the best SPIQ energies, respectively. The shaded areas denote std across three seeds. (b) Ablation study with and without incremental horizon curriculum, showing CRiSP accuracy. (c) Initialization accuracy for VQE tasks. For (b) and (c), the bar indicates the average accuracy, the error bar displays std, and the points correspond to results from three independent runs.

erage) and  $3.63\times$  (best) on MedicalDense tasks. Notably, even on MedicalSparse tasks—where extreme landscape sparsity makes it inherently difficult for either method to discover non-zero reward configurations—CRiSP still realizes GeoMean advantages of  $1.70\times$  (average) and  $1.71\times$  (best) higher accuracy than SPIQ across all instances.

For the MedicalSparse tasks specifically, we observe a wider accuracy distribution among different random seeds, with certain CRiSP instances occasionally underperforming SPIQ. While consistent outperformance across all seeds is ideal, identifying even a single high-quality solution holds immense practical value in realistic quantum computing use cases, as it drastically reduces subsequent quantum resource expenditures. Consequently, the fact that the best-performing seeds consistently originate from CRiSP is of greater practical utility than strictly outperforming the baseline on average. We hypothesize that performance on these sparse tasks is primarily bottlenecked by the inherent difficulty of initial exploration rather than the search policy itself. This is evidenced by the substantially larger performance margins that CRiSP demonstrates on denser benchmarks, where non-zero reward signals become more readily available to guide learning.

Finally, the performance gap between the two methods notably widens as problem dimensionality scales. While SPIQ degrades significantly on larger instances, CRiSP exhibits strong scalability, maintaining average energy accuracies above 92% throughout all Knapsack and MedicalDense benchmarks. This consistent improvement is further corroborated by the convergence behavior illustrated in Fig. 4(a), which confirms that CRiSP progressively and reliably converges toward low-energy (high-return) configurations given sufficient training budgets.

### 4.3 Ablation study on incremental horizon curriculum

To examine the contribution of the incremental horizon curriculum, we test CRiSP with and without the curriculum on two representative benchmarks where the total episode length is large and the energy landscape is highly barren, namely MedicalDense\_14 and MedicalSparse\_20. Due to the substantial computational cost of full-horizon training on MedicalDense tasks, the ablation is conducted under a reduced setting with 3,000 training episodes, a simulation count of 30 for both the warmup and standard phases, and a learning rate of  $3 \times 10^{-4}$ , while keeping all other hyperparameters the same as the configuration for the main results. Both variants are evaluated under this same setting to ensure a fair comparison. The ablation for MedicalSparse\_20 is performed using the identical experimental setup as the main experiments.

As shown in Fig. 4(b), without the curriculum, CRiSP struggles to effectively explore the full search space within the allocated training budget, causing substantial performance degradation on both benchmarks. On MedicalDense\_14, the curriculum pushes the average accuracy from 46.14% to 84.59%. This indicates that the gradual expansion of the search horizon enables the agent to uncover

partially promising configurations in the early stages of training, and to further focus its exploration on those regions as the horizon extends toward its full length. The performance gap becomes even more drastic on `MedicalSparse_20`, where the reward landscape is extremely sparse. Here, the mean accuracy improves  $7.62\times$ , from 5.92% to 45.11%, because the curriculum allows the agent to find positive reward signals during early episodes within confined search spaces—regions that would otherwise remain unexplored during full-horizon exploration. These results confirm that the incremental horizon curriculum is highly beneficial in addressing tasks with large parameter counts and challenging energy landscapes.

#### 4.4 Generalization to VQE

To investigate the applicability of CRiSP beyond the QAOA domain, we preliminarily evaluate the framework on VQE benchmarks using two physical models: the one-dimensional Transverse-Field Ising Model (TFIM) [73] and the XXZ model [9], a specific variant of the Heisenberg model. Detailed Hamiltonian formulations for these models are provided in Section C.5. Both models are evaluated at  $N = 10$  across three coupling strengths,  $J \in \{0.5, 1.0, 2.0\}$ .

We compare CRiSP against a scalable variant of CAFQA [78] (implemented via a GA, as employed in Clapton [86]), a Clifford initialization method designed for VQE, under equal circuit evaluation budgets. Both approaches utilize a circular hardware-efficient ansatz [47] with one repetition, resulting in 40 parameters per circuit. Given the exploratory nature of this experiment, we adopt the closest QAOA benchmark configuration of comparable problem size without VQE-tailored algorithmic setup, performing a grid search over the per-round training epochs  $K \in \{12, 16, 20, 24\}$  and the value coefficient  $c_v \in \{1, 2\}$ .

As presented in Fig. 4(c), CRiSP achieves comparable or higher accuracy than CAFQA across all benchmarks, with GeoMeans of  $1.1\times$  in average accuracy and  $1.11\times$  in best-achieved accuracy (see Appendix B for details). On `Ising_0.5` and `Ising_2.0`, CRiSP consistently outperforms CAFQA by  $1.18\times$  and  $1.29\times$ , respectively. On the XXZ models, although the variance across seeds increases with the coupling strength  $J$ , CRiSP successfully identifies the best circuit configurations across all benchmarks, some of which remain unreachable by CAFQA. While additional hyperparameter tuning would likely further enhance performance, these preliminary results indicate that CRiSP generalizes to VQE settings without requiring task-specific modifications, supporting its potential applicability to a broader class of VQA problems.

## 5 Conclusions, limitations, and future outlook

In this work, we addressed the substantial resource bottleneck of VQA in intermediate-term quantum computing by introducing CRiSP, a reinforcement learning framework for classically simulable quantum state preparation. By formalizing discrete Clifford initialization as a sequential decision-making problem, CRiSP leverages Neural-Guided Monte Carlo Tree Search and a Transformer-based policy to systematically navigate the vast combinatorial search space. Evaluated on a diverse suite of benchmarks, our approach demonstrates robust scalability and consistently outperforms existing state-of-the-art heuristic methods, drastically reducing the initial energy expectation value of parameterized quantum circuits under equivalent computational budgets.

While our framework significantly improves VQA initialization, we note a few important limitations. First, there is no strict mathematical guarantee that lower initial energy deterministically leads to superior convergence or better results after continuous parameter optimization. Nevertheless, considerable empirical evidence from prior literature strongly supports this correlation [6]. Second, like many near-term algorithms, there are no definitive guarantees that VQAs will achieve practical quantum advantage over advanced classical methods. However, their noise resilience and flexibility justify continued pursuit. Finally, regarding scalability, although our curriculum approach handles large parameter counts effectively, the combinatorial explosion of the Clifford search space inevitably imposes a heavy computational burden on classical simulation and training as system sizes scale.

Building upon these insights, we identify four highly promising directions for future research:

**Landscape-aware initialization:** Beyond minimizing energy, future reward signals could incorporate landscape properties (e.g., gradient or Hessian magnitudes). This would guide the agent toward low-energy initial states in highly trainable regions, accelerating convergence to the ground state.

**Near-Clifford state preparation:** Extending the search to include a restricted budget of non-Clifford gates (e.g., T gates) significantly expands the discrete state space. Developing RL frameworks to handle this near-Clifford action space promises much higher-quality classical state preparations.

**Generalization beyond VQAs:** By replacing the Hamiltonian energy objective with unitary similarity metrics, our sequential construction framework can be readily adapted for approximate state preparation or circuit compilation, targeting reductions in T-count or multi-qubit entangling gates.

**Quantum-in-the-loop exploration:** Integrating quantum hardware directly into the optimization loop unlocks states well beyond the Clifford bound. Given the high cost of quantum execution, developing sample-efficient RL for this limited-shot regime is a compelling future direction.

## Acknowledgments and Disclosure of Funding

This material is based upon work supported by the U.S. Department of Energy, Office of Science, Office of Advanced Scientific Computing Research, Accelerated Research in Quantum Computing under Award Number DE-SC0025633. This research used resources of the National Energy Research Scientific Computing Center, a DOE Office of Science User Facility supported by the Office of Science of the U.S. Department of Energy under Contract No. DE-AC02-05CH11231 using NERSC award NERSC DDR-ERCAP0035341. This research was, in part, funded by the U.S. Government. The views and conclusions contained in this document are those of the authors and should not be interpreted as representing the official policies, either expressed or implied, of the U.S. Government.

## References

- [1] Scott Aaronson and Daniel Gottesman. Improved simulation of stabilizer circuits. *Physical Review A—Atomic, Molecular, and Optical Physics*, 70(5):052328, 2004.
- [2] Martin Anthony, Endre Boros, Yves Crama, and Aritanan Gruber. Quadraticization of higher degree pseudo-boolean functions. In *International Conference on Integer Programming and Combinatorial Optimization*, pages 458–469. Springer, 2017. doi: 10.1007/978-3-319-59250-3\_37.
- [3] Jimmy Lei Ba, Jamie Ryan Kiros, and Geoffrey E Hinton. Layer normalization. *arXiv preprint arXiv:1607.06450*, 2016.
- [4] Boaz Barak, Ankur Moitra, Ryan O’Donnell, Prasad Raghavendra, Oded Regev, David Steurer, Luca Trevisan, Aravindan Vijayaraghavan, David Witmer, and John Wright. Beating the random assignment on constraint satisfaction problems of bounded degree. *arXiv*, August 2015. doi: 10.48550/arXiv.1505.03424.
- [5] Yoshua Bengio, Jérôme Louradour, Ronan Collobert, and Jason Weston. Curriculum learning. In *Proceedings of the 26th annual international conference on machine learning*, pages 41–48, 2009.
- [6] Dhanvi Bharadwaj, Yuewen Hou, Guang-Yi Li, and Gokul Subramanian Ravi. Scalable clifford-based classical initialization for the quantum approximate optimization algorithm. *arXiv preprint arXiv:2602.14327*, 2026.
- [7] Jacob Biamonte, Peter Wittek, Nicola Pancotti, Patrick Rebentrost, Nathan Wiebe, and Seth Lloyd. Quantum machine learning. *Nature*, 549(7671):195–202, 2017.
- [8] Kostas Blekos, Dean Brand, Andrea Ceschini, Chiao-Hui Chou, Rui-Hao Li, Komal Pandya, and Alessandro Summer. A review on quantum approximate optimization algorithm and its variants. *Physics Reports*, 1068:1–66, 2024.
- [9] F Bonechi, E Celeghini, R Giachetti, E Sorace, and M Tarlini. Heisenberg xxz model and quantum galilei group. *Journal of Physics A: Mathematical and General*, 25(15):L939, aug 1992. doi: 10.1088/0305-4470/25/15/007. URL <https://dx.doi.org/10.1088/0305-4470/25/15/007>.
- [10] Endre Boros and Peter L. Hammer. Pseudo-boolean optimization. *Discrete Applied Mathematics*, 123(1-3):155–225, 2002. doi: 10.1016/S0166-218X(01)00341-9.

- [11] Endre Boros, Peter L Hammer, and Gabriel Tavares. Local search heuristics for quadratic unconstrained binary optimization (qubo). *Journal of Heuristics*, 13(2):99–132, 2007.
- [12] Sergey Bravyi and Alexei Kitaev. Universal quantum computation with ideal clifford gates and noisy ancillas. *Physical Review A—Atomic, Molecular, and Optical Physics*, 71(2):022316, 2005.
- [13] Cameron B Browne, Edward Powley, Daniel Whitehouse, Simon M Lucas, Peter I Cowling, Philipp Rohlfshagen, Stephen Tavener, Diego Perez, Spyridon Samothrakis, and Simon Colton. A survey of monte carlo tree search methods. *IEEE Transactions on Computational Intelligence and AI in games*, 4(1):1–43, 2012.
- [14] Marco Cerezo, Andrew Arrasmith, Ryan Babbush, Simon C Benjamin, Suguru Endo, Keisuke Fujii, Jarrod R McClean, Kosuke Mitarai, Xiao Yuan, Lukasz Cincio, et al. Variational quantum algorithms. *Nature Reviews Physics*, 3(9):625–644, 2021.
- [15] MH Cheng, KE Khosla, CN Self, M Lin, BX Li, AC Medina, and MS Kim. Clifford circuit initialization for variational quantum algorithms. *Physical Review A*, 111(6):062413, 2025.
- [16] Chi-Ning Chou, Peter J. Love, Juspreet Singh Sandhu, and Jonathan Shi. Limitations of Local Quantum Algorithms on Random Max-k-XOR and Beyond, February 2022.
- [17] Barry A. Cipra. An introduction to the ising model. *The American Mathematical Monthly*, 94(10):937–959, 1987. doi: 10.1080/00029890.1987.12000742. URL <https://doi.org/10.1080/00029890.1987.12000742>.
- [18] Siddharth Dangwal, Gokul Subramanian Ravi, Poulami Das, Kaitlin N. Smith, Jonathan M. Baker, and Frederic T. Chong. Varsaw: Application-tailored measurement error mitigation for variational quantum algorithms, 2023.
- [19] E. Farhi, J. Goldstone, and S. Gutmann. A Quantum Approximate Optimization Algorithm Applied to a Bounded Occurrence Constraint Problem. *arXiv*, June 2015. doi: 10.48550/arXiv.1412.6062.
- [20] Bryan Eastin and Emanuel Knill. Restrictions on transversal encoded quantum gate sets. *Physical review letters*, 102(11):110502, 2009.
- [21] Jeffrey M Epstein, Andrew W Cross, Easwar Magesan, and Jay M Gambetta. Investigating the limits of randomized benchmarking protocols. *Physical Review A*, 89(6):062321, 2014.
- [22] Edward Farhi, Jeffrey Goldstone, and Sam Gutmann. A quantum approximate optimization algorithm. *arXiv preprint arXiv:1411.4028*, 2014.
- [23] Edward Farhi, Jeffrey Goldstone, Sam Gutmann, and Leo Zhou. The Quantum Approximate Optimization Algorithm and the Sherrington-Kirkpatrick Model at Infinite Size. *Quantum*, 6:759, July 2022. ISSN 2521-327X. doi: 10.22331/q-2022-07-07-759.
- [24] Alhussein Fawzi, Matej Balog, Aja Huang, Thomas Hubert, Bernardino Romera-Paredes, Mohammadamin Barekatin, Alexander Novikov, Francisco J R. Ruiz, Julian Schrittwieser, Grzegorz Swirszcz, et al. Discovering faster matrix multiplication algorithms with reinforcement learning. *Nature*, 610(7930):47–53, 2022.
- [25] Fuchang Gao and Lixing Han. Implementing the nelder-mead simplex algorithm with adaptive parameters. *Comput. Optim. Appl.*, 51(1):259–277, January 2012. ISSN 0926-6003. doi: 10.1007/s10589-010-9329-3. URL <https://doi.org/10.1007/s10589-010-9329-3>.
- [26] Craig Gidney. Stim: a fast stabilizer circuit simulator. *Quantum*, 5:497, July 2021. ISSN 2521-327X. doi: 10.22331/q-2021-07-06-497. URL <https://doi.org/10.22331/q-2021-07-06-497>.
- [27] Craig Gidney, Noah Shutty, and Cody Jones. Magic state cultivation: growing t states as cheap as cnot gates. *arXiv preprint arXiv:2409.17595*, 2024.

- [28] Tudor Giurgica-Tiron, Yousef Hindy, Ryan LaRose, Andrea Mari, and William J Zeng. Digital zero noise extrapolation for quantum error mitigation. In *2020 IEEE International Conference on Quantum Computing and Engineering (QCE)*, pages 306–316. IEEE, 2020.
- [29] Fred Glover, Gary Kochenberger, and Yu Du. A tutorial on formulating and using qubo models. *arXiv preprint arXiv:1811.11538*, 2019. URL <https://arxiv.org/abs/1811.11538>.
- [30] Google. Google quantum computing roadmap. <https://quantumai.google/roadmap>, 2024. Accessed: 2024-11-22.
- [31] Daniel Gottesman. The heisenberg representation of quantum computers. *arXiv preprint quant-ph/9807006*, 1998.
- [32] Edward Grant, Leonard Wossnig, Mateusz Ostaszewski, and Marcello Benedetti. An initialization strategy for addressing barren plateaus in parametrized quantum circuits. *Quantum*, 3:214, 2019.
- [33] Harper R. Grimsley, Sophia E. Economou, Edwin Barnes, and Nicholas J. Mayhall. An adaptive variational algorithm for exact molecular simulations on a quantum computer. *Nature Communications*, 10(1), Jul 2019. ISSN 2041-1723. doi: 10.1038/s41467-019-10988-2. URL <http://dx.doi.org/10.1038/s41467-019-10988-2>.
- [34] Lov K Grover. A fast quantum mechanical algorithm for database search. In *Proceedings of the twenty-eighth annual ACM symposium on Theory of computing*, pages 212–219, 1996.
- [35] Gurobi Optimization, LLC. Gurobi Optimizer Reference Manual, 2024. URL <https://www.gurobi.com>.
- [36] Stuart Hadfield, Zihui Wang, Bryan O’Gorman, Eleanor G. Rieffel, Davide Venturelli, and Rupak Biswas. From the Quantum Approximate Optimization Algorithm to a Quantum Alternating Operator Ansatz. *Algorithms*, 12(2):34, February 2019. doi: 10.3390/a12020034.
- [37] Tianyi Hao, Amanda Xu, and Swamit Tannu. Reducing t gates with unitary synthesis. *arXiv preprint arXiv:2503.15843*, 2025.
- [38] Charles R Harris, K Jarrod Millman, Stéfan J Van Der Walt, Ralf Gommers, Pauli Virtanen, David Cournapeau, Eric Wieser, Julian Taylor, Sebastian Berg, Nathaniel J Smith, et al. Array programming with numpy. *nature*, 585(7825):357–362, 2020.
- [39] M. B. Hastings. Classical and Quantum Bounded Depth Approximation Algorithms. *arXiv*, August 2019. doi: 10.48550/arXiv.1905.07047.
- [40] Dan Hendrycks and Kevin Gimpel. Gaussian error linear units (gelus). *arXiv preprint arXiv:1606.08415*, 2016.
- [41] Rebekah Herrman, Phillip C Lotshaw, James Ostrowski, Travis S Humble, and George Siopsis. Multi-angle quantum approximate optimization algorithm. *Scientific Reports*, 12(1):6781, 2022.
- [42] Peter J Huber. Robust estimation of a location parameter. In *Breakthroughs in statistics: Methodology and distribution*, pages 492–518. Springer, 1992.
- [43] IBM. *IBM ILOG CPLEX Optimization Studio*, 2024. <https://www.ibm.com/products/ilog-cplex-optimization-studio>.
- [44] IBM. Ibm quantum computing roadmap. <https://www.ibm.com/roadmaps/quantum>, 2024. Accessed: 2024-11-22.
- [45] J. Preskill. Beyond nisq: The megaquop machine. *ACM Transactions on Quantum Computing*, 6(3):1–7, April 2025. ISSN 2643-6817. doi: 10.1145/3723153. URL <http://dx.doi.org/10.1145/3723153>.

- [46] Yuwei Jin, Zirui Li, Fei Hua, Tianyi Hao, Huiyang Zhou, Yipeng Huang, and Eddy Z Zhang. Tetris: A compilation framework for vqa applications in quantum computing. In *2024 ACM/IEEE 51st Annual International Symposium on Computer Architecture (ISCA)*, pages 277–292. IEEE, 2024.
- [47] Abhinav Kandala, Antonio Mezzacapo, Kristan Temme, Maika Takita, Markus Brink, Jerry M Chow, and Jay M Gambetta. Hardware-efficient variational quantum eigensolver for small molecules and quantum magnets. *Nature*, 549(7671):242–246, 2017.
- [48] Amara Katarbarwa, Katerina Gratsea, Athena Caesura, and Peter D. Johnson. Early fault-tolerant quantum computing. *PRX Quantum*, 5:020101, Jun 2024. doi: 10.1103/PRXQuantum.5.020101. URL <https://link.aps.org/doi/10.1103/PRXQuantum.5.020101>.
- [49] Youngseok Kim, Andrew Eddins, Sajant Anand, Ken Xuan Wei, Ewout Van Den Berg, Sami Rosenblatt, Hasan Nayfeh, Yantao Wu, Michael Zaletel, Kristan Temme, and Abhinav Kandala. Evidence for the utility of quantum computing before fault tolerance. *Nature*, 618(7965): 500–505, 2023.
- [50] Diederik P. Kingma and Jimmy Ba. Adam: A method for stochastic optimization, 2017. URL <https://arxiv.org/abs/1412.6980>.
- [51] Vadym Kliuchnikov, Dmitri Maslov, and Michele Mosca. Fast and efficient exact synthesis of single qubit unitaries generated by clifford and t gates. *arXiv preprint arXiv:1206.5236*, 2012.
- [52] Gary Kochenberger, Jin-Kao Hao, Fred Glover, Mark Lewis, Zhipeng Lü, Haibo Wang, and Yang Wang. The unconstrained binary quadratic programming problem: a survey. *Journal of Combinatorial Optimization*, 28:58–81, 2014. doi: 10.1007/s10878-014-9734-0.
- [53] David Kremer, Ali Javadi-Abhari, and Priyanka Mukhopadhyay. Optimizing the non-clifford-count in unitary synthesis using reinforcement learning. *arXiv preprint arXiv:2509.21709*, 2025.
- [54] Wim Lavrijsen, Ana Tudor, Juliane Müller, Costin Iancu, and Wibe de Jong. Classical optimizers for noisy intermediate-scale quantum devices. In *2020 IEEE International Conference on Quantum Computing and Engineering (QCE)*, pages 267–277, 2020. doi: 10.1109/QCE49297.2020.00041.
- [55] Xinwei Lee, Ningyi Xie, Dongsheng Cai, Yoshiyuki Saito, and Nobuyoshi Asai. A Depth-Progressive Initialization Strategy for Quantum Approximate Optimization Algorithm. *Mathematics*, 11(9):2176, 2023. doi: 10.3390/math11092176.
- [56] Xinwei Lee, Xinjian Yan, Ningyi Xie, Dongsheng Cai, Yoshiyuki Saito, and Nobuyoshi Asai. Iterative layerwise training for the quantum approximate optimization algorithm. *Physical Review A*, 109(5):052406, 2024.
- [57] Gushu Li, Anbang Wu, Yunong Shi, Ali Javadi-Abhari, Yufei Ding, and Yuan Xie. Paulihedral: a generalized block-wise compiler optimization framework for quantum simulation kernels. In *Proceedings of the 27th ACM International Conference on Architectural Support for Programming Languages and Operating Systems*, pages 554–569, 2022.
- [58] Cedric Yen-Yu Lin and Yechao Zhu. Performance of QAOA on Typical Instances of Constraint Satisfaction Problems with Bounded Degree. *arXiv*, January 2016. doi: 10.48550/arXiv.1601.01744.
- [59] Daniel Litinski. Magic state distillation: Not as costly as you think. *Quantum*, 3:205, 2019.
- [60] Ilya Loshchilov and Frank Hutter. Decoupled weight decay regularization. *arXiv preprint arXiv:1711.05101*, 2017.
- [61] Anqi Mao, Mehryar Mohri, and Yutao Zhong. Cross-entropy loss functions: Theoretical analysis and applications. In *International conference on Machine learning*, pages 23803–23828. pmlr, 2023.

- [62] Kunal Marwaha. Local classical MAX-CUT algorithm outperforms QAOA on high-girth regular graphs. *Quantum*, 5, April 2021. ISSN 2521-327X. doi: 10.22331/q-2021-04-20-437.
- [63] Nina Mazyavkina, Sergey Sviridov, Sergei Ivanov, and Evgeny Burnaev. Reinforcement learning for combinatorial optimization: A survey. *Computers & Operations Research*, 134: 105400, 2021.
- [64] Jarrod R McClean, Jonathan Romero, Ryan Babbush, and Alán Aspuru-Guzik. The theory of variational hybrid quantum-classical algorithms. *New Journal of Physics*, 18(2):023023, 2016.
- [65] Jarrod R McClean, Sergio Boixo, Vadim N Smelyanskiy, Ryan Babbush, and Hartmut Neven. Barren plateaus in quantum neural network training landscapes. *Nat. Commun.*, 9(1):4812, 2018.
- [66] Nikolaj Moll, Panagiotis Barkoutsos, Lev Bishop, Jerry Chow, Andrew Cross, Daniel Egger, Stefan Filipp, Andreas Fuhrer, Jay Gambetta, Marc Ganzhorn, Abhinav Kandala, Antonio Mezzacapo, Peter Müller, Walter Riess, Gian Salis, John Smolin, Ivano Tavernelli, and Kristan Temme. Quantum optimization using variational algorithms on near-term quantum devices. *Quantum Science and Technology*, 3, 06 2018. doi: 10.1088/2058-9565/aab822.
- [67] Michael A. Nielsen and Isaac L. Chuang. *Quantum Computation and Quantum Information: 10th Anniversary Edition*. Cambridge University Press, 2010.
- [68] Julius Beneoluchi Odili. Combinatorial optimization in science and engineering. *Current Science*, pages 2268–2274, 2017.
- [69] Joe O’Gorman and Earl T. Campbell. Quantum computation with realistic magic-state factories. *Physical Review A*, 95(3), Mar 2017. ISSN 2469-9934. doi: 10.1103/physreva.95.032338. URL <http://dx.doi.org/10.1103/PhysRevA.95.032338>.
- [70] Seohong Park, Kevin Frans, Deepinder Mann, Benjamin Eysenbach, Aviral Kumar, and Sergey Levine. Horizon reduction makes rl scalable. *arXiv preprint arXiv:2506.04168*, 2025.
- [71] Adam Paszke, Sam Gross, Francisco Massa, Adam Lerer, James Bradbury, Gregory Chanan, Trevor Killeen, Zeming Lin, Natalia Gimelshein, Luca Antiga, et al. Pytorch: An imperative style, high-performance deep learning library. *Advances in neural information processing systems*, 32, 2019.
- [72] Alberto Peruzzo, Jarrod McClean, Peter Shadbolt, Man-Hong Yung, Xiao-Qi Zhou, Peter J Love, Alán Aspuru-Guzik, and Jeremy L O’Brien. A variational eigenvalue solver on a photonic quantum processor. *Nature communications*, 5:4213, 2014.
- [73] Pierre Pfeuty. The one-dimensional ising model with a transverse field. *ANNALS of Physics*, 57(1):79–90, 1970.
- [74] John Preskill. Quantum computing in the nisq era and beyond. *Quantum*, 2:79, 2018.
- [75] Qiskit contributors. Qiskit: An open-source framework for quantum computing, 2023.
- [76] Ronald L Rardin. *Optimization in operations research*, volume 166. Prentice Hall Upper Saddle River, NJ, 1998.
- [77] Gokul Subramanian Ravi, Kaitlin N. Smith, Pranav Gokhale, Andrea Mari, Nathan Earnest, Ali Javadi-Abhari, and Frederic T. Chong. Vaqem: A variational approach to quantum error mitigation, 2021.
- [78] Gokul Subramanian Ravi, Pranav Gokhale, Yi Ding, William Kirby, Kaitlin Smith, Jonathan M Baker, Peter J Love, Henry Hoffmann, Kenneth R Brown, and Frederic T Chong. Cafqa: A classical simulation bootstrap for variational quantum algorithms. In *Proceedings of the 28th ACM International Conference on Architectural Support for Programming Languages and Operating Systems, Volume 1*, pages 15–29, 2022.

- [79] Gokul Subramanian Ravi, Kaitlin N. Smith, Jonathan M. Baker, Tejas Kannan, Nathan Earnest, Ali Javadi-Abhari, Henry Hoffmann, and Frederic T. Chong. Navigating the dynamic noise landscape of variational quantum algorithms with qismet, 2022. URL <https://arxiv.org/abs/2209.12280>.
- [80] A. H. G. Rinnooy Kan and G. T. Timmer. Stochastic global optimization methods part i: Clustering methods. *Mathematical Programming*, 39:27–56, 1987.
- [81] Neil J Ross and Peter Selinger. Optimal ancilla-free clifford+ t approximation of z-rotations. *Quantum Inf. Comput.*, 16(11&12):901–953, 2016.
- [82] Francisco JR Ruiz, Tuomas Laakkonen, Johannes Bausch, Matej Balog, Mohammadamin Berekatain, Francisco JH Heras, Alexander Novikov, Nathan Fitzpatrick, Bernardino Romera-Paredes, John Van De Wetering, et al. Quantum circuit optimization with alphasensor. *Nature Machine Intelligence*, 7(3):374–385, 2025.
- [83] Stefan H. Sack and Maksym Serbyn. Quantum annealing initialization of the quantum approximate optimization algorithm. *Quantum*, 5:491, July 2021. ISSN 2521-327X. doi: 10.22331/q-2021-07-01-491. URL <http://dx.doi.org/10.22331/q-2021-07-01-491>.
- [84] Stefan H Sack and Maksym Serbyn. Quantum annealing initialization of the quantum approximate optimization algorithm. *quantum*, 5:491, 2021.
- [85] Abdelkader Sbihi and Richard W Eglese. Combinatorial optimization and green logistics. *Annals of Operations Research*, 175(1):159–175, 2010.
- [86] Lennart Maximilian Seifert, Siddharth Dangwal, Frederic T Chong, and Gokul Subramanian Ravi. Clapton: Clifford assisted problem transformation for error mitigation in variational quantum algorithms. In *Proceedings of the 29th ACM International Conference on Architectural Support for Programming Languages and Operating Systems, Volume 4*, pages 47–62, 2024.
- [87] Dhirpal Shah, Mariesa Teo, Ryan A. Robinett, Sophia Madejski, Zachary Morrell, Siddhi Ramesh, Colin Campbell, Bharath Thotakura, Victory Omole, Ben Hall, Aram W. Harrow, Teague Tomesh, Alexander T. Pearson, Frederic T. Chong, and Samantha J. Riesenfeld. Toward quantum-enabled biomarker discovery: An outlook from q4bio, 2025. URL <https://arxiv.org/abs/2509.25904>.
- [88] Peter W Shor. Fault-tolerant quantum computation. In *Proceedings of 37th conference on foundations of computer science*, pages 56–65. IEEE, 1996.
- [89] Peter W. Shor. Polynomial-time algorithms for prime factorization and discrete logarithms on a quantum computer. *SIAM Journal on Computing*, 26(5):1484–1509, Oct 1997. ISSN 1095-7111. doi: 10.1137/s0097539795293172. URL <http://dx.doi.org/10.1137/S0097539795293172>.
- [90] David Silver, Julian Schrittwieser, Karen Simonyan, Ioannis Antonoglou, Aja Huang, Arthur Guez, Thomas Hubert, Lucas Baker, Matthew Lai, Adrian Bolton, et al. Mastering the game of go without human knowledge. *nature*, 550(7676):354–359, 2017.
- [91] Volodymyr Sivak, Alexis Morvan, Michael Broughton, Matthew Neeley, Alec Eickbusch, Dmitry Abanin, Amira Abbas, Rajeev Acharya, Laleh Aghababaie Beni, Georg Aigeldinger, et al. Reinforcement learning control of quantum error correction. *arXiv preprint arXiv:2511.08493*, 2025.
- [92] James C Spall. Multivariate stochastic approximation using a simultaneous perturbation gradient approximation. *IEEE transactions on automatic control*, 37(3):332–341, 2002.
- [93] Michael Streif and Martin Leib. Training the quantum approximate optimization algorithm without access to a quantum processing unit. *IOP*, 5(3):034008, May 2020. ISSN 2058-9565. doi: 10.1088/2058-9565/ab8c2b. Publisher: IOP Publishing.
- [94] Richard S Sutton, Andrew G Barto, et al. *Introduction to reinforcement learning*, volume 135. MIT press Cambridge, 1998.

- [95] Jules Tilly, Hongxiang Chen, Shuxiang Cao, Dario Picozzi, Kanav Setia, Ying Li, Edward Grant, Leonard Wossnig, Ivan Rungger, George H. Booth, and Jonathan Tennyson. The variational quantum eigensolver: A review of methods and best practices. *Physics Reports*, 986:1–128, 2022. ISSN 0370-1573. doi: <https://doi.org/10.1016/j.physrep.2022.08.003>. URL <https://www.sciencedirect.com/science/article/pii/S0370157322003118>. The Variational Quantum Eigensolver: a review of methods and best practices.
- [96] Matthew Treinish, Ivan Carvalho, Georgios Tsilimigkounakis, and Nahum Sá. rustworkx: A high-performance graph library for python. *arXiv preprint arXiv:2110.15221*, 2021.
- [97] Ashish Vaswani, Noam Shazeer, Niki Parmar, Jakob Uszkoreit, Llion Jones, Aidan N Gomez, Łukasz Kaiser, and Illia Polosukhin. Attention is all you need. *Advances in neural information processing systems*, 30, 2017.
- [98] Hanrui Wang, Yongshan Ding, Jiaqi Gu, Zirui Li, Yujun Lin, David Z. Pan, Frederic T. Chong, and Song Han. Quantumnas: Noise-adaptive search for robust quantum circuits, 2022.
- [99] Samson Wang, Piotr Czarnik, Andrew Arrasmith, Marco Cerezo, Lukasz Cincio, and Patrick J Coles. Can error mitigation improve trainability of noisy variational quantum algorithms? *arXiv preprint arXiv:2109.01051*, 2021.
- [100] Zhihui Wang, Stuart Hadfield, Zhang Jiang, and Eleanor G. Rieffel. Quantum Approximate Optimization Algorithm for MaxCut: A Fermionic View. *Physical Review A*, 97(2):022304, February 2018. ISSN 2469-9926, 2469-9934. doi: 10.1103/PhysRevA.97.022304.
- [101] Mathias Weiden, Justin Kallor, John Kubiawicz, and Costin Iancu. Making neural networks more suitable for approximate clifford+ t circuit synthesis. In *2025 IEEE International Conference on Quantum Computing and Engineering (QCE)*, volume 1, pages 501–510. IEEE, 2025.
- [102] Jiahao Yao, Haoya Li, Marin Bukov, Lin Lin, and Lexing Ying. Monte carlo tree search based hybrid optimization of variational quantum circuits. In *Mathematical and Scientific Machine Learning*, pages 49–64. PMLR, 2022.
- [103] Z. Zhang. PRIMA: Reference Implementation for Powell’s Methods with Modernization and Amelioration. available at <http://www.libprima.net>, DOI: 10.5281/zenodo.8052654, 2023.
- [104] Leo Zhou, Sheng-Tao Wang, Soonwon Choi, Hannes Pichler, and Mikhail D. Lukin. Quantum approximate optimization algorithm: Performance, mechanism, and implementation on near-term devices. *Phys. Rev. X*, 10:021067, Jun 2020. doi: 10.1103/PhysRevX.10.021067. URL <https://link.aps.org/doi/10.1103/PhysRevX.10.021067>.
- [105] Ciyou Zhu, Richard H. Byrd, Peihuang Lu, and Jorge Nocedal. Algorithm 778: L-bfgs-b: Fortran subroutines for large-scale bound-constrained optimization. *ACM Trans. Math. Softw.*, 23(4):550–560, December 1997. ISSN 0098-3500. doi: 10.1145/279232.279236. URL <https://doi.org/10.1145/279232.279236>.

# Appendices

## A Further experimental details

The implementation uses Qiskit 2.3.0 [75] for general quantum circuit operations, Pytorch 2.5.1 [71] for model training, Stim 1.15.0 [26] for classical stabilizer tableau simulation to compute the expected energy of the synthesized quantum circuits, NumPy 2.3.3 [38] for numerical computation, and rustworkx 0.17.1 [96] for graph operations, all running on Python 3.12. All experiments are conducted on a single NVIDIA A100 GPU with a 64-core AMD EPYC 7763 CPU and up to 64GB memory. Execution time ranges from 10 hours to over one week, depending on the simulation scale and budget. Hyperparameters are reported in Table 1. For VQE experiments, the values of  $K$  and  $c_v$  are listed in Table 2, with all remaining hyperparameters set to MaxCut\_8 configuration in Table 1.

Table 1: Hyperparameters for CRiSP training and architecture. When indicating benchmarks, MC, Kn, MD, and MS refer to MaxCut, Knapsack, MedicalDense, and MedicalSparse, respectively.

Category	Hyperparameter	Value
Architecture	Transformer layers / heads	2 / 4
	Transformer input / FF dimension	128 / 256
	State / Positional embedding dimension	32 / 96
	Positional embedding	Sinusoidal [97]
	Hamiltonian embedding size	[256, 128]
	Policy / Value head size	[128, 128, 24] / [256, 128, 64, 1]
	Context length ( $c_{ctx}$ )	64
	Activation / Normalization	GELU [40] / LayerNorm [3]
MCTS	$c_{puct}$	1.0 (default), 0.8 (MD_12/14/20), 1.5 (MS_15_1)
	Dirichlet noise ( $\alpha_D, \epsilon_D$ )	0.15, 0.2 (Eval: 0.15, 0.1)
	Warmup / Standard simulations ( $m$ )	50 / 100 (default), 30 / 50 (MC_20, Kn_16, MD_12/14/20)
	Parallel workers	30
	Initial / Decayed temperature $\tau$	1.0 / 0.75
Optimization	Total episodes	$6 \times 10^4$ (default), $3 \times 10^4$ (MC_20, Kn_12/16, MD_12), $1.5 \times 10^4$ (MD_14), $6 \times 10^3$ (MD_20)
	Training epochs ( $K$ )	16 (default), 12 (MC_8), 24 (MC_20, Kn_9/12/16), 32 (MD_12/14), 40 (MD_20)
	Optimizer	AdamW [60]
	Peak learning rate	$10^{-4}$ (default), $3 \times 10^{-4}$ (MD_20)
	Weight decay	$10^{-6}$
	Value coefficient ( $c_v$ )	2.0
	Mini-batch size	1024 (default), 512 (MC_8/12, Kn_4, MS_15_1/15_2)
	Gradient clipping	1.0
	Replay buffer size	$5 \times 10^5$ (default), $10^5$ (MC_20, Kn_9/12/16, MD_12, MS_20), $1.5 \times 10^5$ (MD_14), $4 \times 10^5$ (MD_20)
	Best game buffer size	$10^3$ (default), $2 \times 10^3$ (MC_20, Kn_9/12), $3 \times 10^3$ (Kn_16, MD_12), $5 \times 10^3$ (MD_14), $10^4$ (MD_20)
Training sample ratio (replay, best game)	(0, 0) (initial), (1.0, 0) (after 300 episodes), (0.9, 0.1) (after 600 episodes)	

Table 2: Hyperparameters for VQE training across different tasks.

Task	Training epochs ( $K$ )	Value coefficient ( $c_v$ )
Ising_0.5	12	1.0
Ising_1.0	16	2.0
Ising_2.0	24	2.0
XXZ_0.5	16	1.0
XXZ_1.0	12	1.0
XXZ_2.0	16	1.0

## B Numerical results for QAOA and VQE benchmarks

Table 3 shows the numerical results for QAOA benchmarks, and the simulation outcomes for VQE tasks are provided in Table 4.

Table 3: QAOA benchmark results.  $n$  and  $N_{\text{params}}$  denote the number of qubits and circuit parameters, respectively.  $E_{\text{opt}}$  represents the ground state energy of the problem. CRiSP and SPIQ are compared under equal circuit evaluation budgets. SPIQ-R denotes SPIQ evaluated with the same number of update rounds as CRiSP. Results are reported as mean  $\pm$  standard deviation (std) across three independent runs.  $\dagger$  indicates tasks where the incremental horizon curriculum is applied. Bold values denote the best average performance for each task.

Category	Task	$n$	$N_{\text{params}}$	$E_{\text{opt}}$	CRiSP (Ours) (%)	SPIQ (%)	SPIQ-R (%)
MaxCut	MaxCut_8	8	36	-46	<b>100</b> $\pm$ 0	83.33 $\pm$ 16.02	86.96 $\pm$ 18.95
	MaxCut_12	12	78	-88	<b>92.42</b> $\pm$ 6.56	47.35 $\pm$ 9.46	51.89 $\pm$ 11.44
	MaxCut_16	16	136	-155	<b>76.56</b> $\pm$ 1.34	33.55 $\pm$ 6.15	37.85 $\pm$ 9.51
	MaxCut_20	20	210	-192	<b>55.9</b> $\pm$ 20.37	4.69 $\pm$ 4.45	9.55 $\pm$ 4.18
Knapsack	Knapsack_4	8	44	-255	<b>99.74</b> $\pm$ 0.45	91.63 $\pm$ 2.27	91.63 $\pm$ 2.27
	Knapsack_9	14	119	-2309.5	<b>94.56</b> $\pm$ 4.15	76.24 $\pm$ 19.86	81.50 $\pm$ 16.75
	Knapsack_12	18	189	-7079.5	<b>92.18</b> $\pm$ 6.59	15.34 $\pm$ 12.83	29.68 $\pm$ 4.87
	Knapsack_16	22	275	-19538.5	<b>93.61</b> $\pm$ 2.85	3.6 $\pm$ 6.23	4.26 $\pm$ 7.2
MedicalDense	MedDense_12 $\dagger$	12	310	-24013.6	<b>99.98</b> $\pm$ 0.01	73.58 $\pm$ 6.36	86.08 $\pm$ 10.49
	MedDense_14 $\dagger$	14	483	-26014.2	<b>96.14</b> $\pm$ 3.84	37.16 $\pm$ 4.44	47.41 $\pm$ 8.88
	MedDense_20 $\dagger$	20	1370	-32023.8	<b>93.71</b> $\pm$ 6.25	2.08 $\pm$ 3.6	4.16 $\pm$ 3.6
MedicalSparse	MedSparse_15_1 $\dagger$	15	83	-0.365	<b>38.81</b> $\pm$ 45.02	21.87 $\pm$ 19.75	24.91 $\pm$ 23.19
	MedSparse_15_2 $\dagger$	15	84	-0.380	<b>83.74</b> $\pm$ 22.56	49.82 $\pm$ 7.31	51.38 $\pm$ 4.74
	MedSparse_20 $\dagger$	20	107	-0.168	<b>45.11</b> $\pm$ 24.96	27.17 $\pm$ 23.11	34.87 $\pm$ 17.46
<b>Overall Mean</b>					<b>83.03</b>	40.53	45.87

Table 4: VQE results on Ising and XXZ models. CRiSP and CAFQA are compared under equal circuit evaluation budgets. Results are reported as mean  $\pm$  std across three independent runs. Bold values indicate the best average performance for each task.

Model	Task	$n$	$N_{\text{param}}$	$E_{\text{opt}}$	CRiSP (Ours) (%)	CAFQA (%)
Ising	Ising_0.5	10	40	-10.570	<b>94.61</b> $\pm$ 0.00	80.42 $\pm$ 0.00
	Ising_1.0	10	40	-12.381	<b>75.38</b> $\pm$ 4.66	<b>75.38</b> $\pm$ 9.33
	Ising_2.0	10	40	-19.531	<b>92.16</b> $\pm$ 0.00	71.68 $\pm$ 0.00
XXZ	XXZ_0.5	10	40	-11.665	<b>77.15</b> $\pm$ 0.00	74.29 $\pm$ 4.95
	XXZ_1.0	10	40	-17.032	<b>74.37</b> $\pm$ 3.39	72.41 $\pm$ 3.39
	XXZ_2.0	10	40	-28.722	<b>75.44</b> $\pm$ 10.64	69.63 $\pm$ 0.00
<b>Overall Mean</b>					<b>77.93</b>	73.97

## C Quantum computing background

### C.1 Qubits, quantum gates, and the Clifford group

At the core of quantum computation lies the quantum bit, or *qubit*. In stark contrast to deterministic classical bits, a single qubit can occupy a linear combination, or superposition, of its computational basis states, denoted mathematically as  $|\psi\rangle = \alpha|0\rangle + \beta|1\rangle$ . This principle scales exponentially: the state of an  $N$ -qubit register is represented by a joint superposition across all  $2^N$  possible classical bitstrings within  $\{0, 1\}^N$ . To evolve these quantum states, one applies continuous unitary transformations referred to as *quantum gates*. Theoretical and experimental focus is frequently directed toward single- and two-qubit operations, as they collectively provide a universal basis capable of executing any arbitrary quantum algorithm [67].

Within quantum information theory, the single-qubit Pauli operators, denoted as  $\mathcal{P} = \{I, X, Y, Z\}$ , serve as a foundational toolkit. The identity matrix  $I$  acts trivially by preserving the state, whereas the

$X$  operator induces a direct bit flip ( $|0\rangle \leftrightarrow |1\rangle$ ). Conversely, the  $Z$  operator functions as a phase flip, appending a negative sign strictly to the excited state ( $Z|1\rangle = -|1\rangle$ ). The  $Y$  gate effectively couples both bit and phase flips, defined as  $Y = iXZ$ . To describe multi-qubit interactions, the  $N$ -qubit Pauli group  $\mathcal{P}_N$  is constructed via the  $N$ -fold tensor product of these fundamental single-qubit operators, such that  $\mathcal{P}_N = \mathcal{P}^{\otimes N}$ .

Expanding on this foundation yields the *Clifford group*  $\mathcal{C}_N$ , a paramount algebraic structure in quantum computing. For an  $N$ -qubit system,  $\mathcal{C}_N$  encompasses all quantum operations  $C$  that act as normalizers for the Pauli group  $\mathcal{P}_N$ . This requirement dictates that mapping a Pauli operator through a Clifford gate must return another valid Pauli operator, expressed mathematically as:

$$CPC^\dagger \in \pm\mathcal{P}_N \quad \forall P \in \mathcal{P}_N. \quad (2)$$

The transformation  $CPC^\dagger$  is formally known as the *conjugation* of a Pauli matrix  $P$  by a Clifford operation  $C$ , which maps to a new Pauli string, potentially with an inverted sign. Because Pauli operators trivially normalize themselves, the Pauli group inherently exists as a strict subgroup within the broader Clifford group ( $\mathcal{P}_N \subset \mathcal{C}_N$ ).

## C.2 Universal quantum gate sets and associated costs

To perform arbitrary quantum computations, a universal gate set is necessary to approximate any unitary operator to a desired precision. In the context of fault-tolerant quantum computing (FTQC), the discrete Clifford+T set is a standard choice. By themselves, Clifford operations—such as the Pauli, Hadamard, and CNOT gates—are non-universal. However, supplementing them with the non-Clifford T gate unlocks universality, allowing for the precise approximation of continuous operations [51]. Tools like Gridsynth [81] are used to compile continuous arbitrary gates into discrete Clifford+T sequences. The drawback is that achieving higher mathematical precision necessitates exponentially longer gate sequences, leading to a massive computational overhead that is especially prohibitive in the early FTQC era.

This bottleneck is a direct consequence of the Eastin-Knill theorem [20], which establishes that no quantum error correction (QEC) code can natively and fault-tolerantly implement a universal gate set. As a result, standard QEC schemes like the surface code can easily protect Clifford operations but fundamentally cannot correct errors for non-Clifford gates such as the T gate or continuous  $R_z(\theta)$  rotations.

To execute these non-Clifford operations, FTQC architectures rely on a resource-intensive procedure known as *magic state distillation* (or T state distillation) [12, 59]. This method generates high-fidelity resource states, such as the T state  $|T\rangle = |0\rangle + \exp(i\frac{\pi}{4})|1\rangle$ . Once prepared, these low-error T states are consumed alongside an arbitrary data qubit to successfully apply a T gate to the circuit, though this process incurs substantial qubit-cycle penalties.

The physical implementation of this process occurs in "magic state factories" [59]. The procedure begins by initializing several surface code patches in the  $|+\rangle = (|0\rangle + |1\rangle)/\sqrt{2}$  state and applying a series of logical rotations. A designated subset of these qubits is then measured to extract an error syndrome. If this signature flags an error during the logical rotations, the entire batch is discarded, and the protocol restarts. If the signature is clear, the remaining unmeasured qubits yield distilled T states. Because the syndrome measurements cannot catch every possible error type, the final T states are of exceptionally high fidelity, but not strictly perfect.

The footprint of a T state distillation protocol is largely defined by its input-to-output patch ratio, alongside the spatial and temporal code distances ( $d_X$ ,  $d_Z$ , and  $d_m$ ). For example, a standard  $(15\text{-to-}1)_{7,3,3}$  factory consumes 15 raw input patches to generate a single distilled T state, utilizing distances of  $d_X = 7$ ,  $d_Z = 3$ , and  $d_m = 3$ . Suppressing the error rate of the output T states requires scaling up these dimensions, which directly inflates the space-time volume of the factory. Consequently, protocols designed for higher output yields—such as a  $(20\text{-to-}4)$  factory—demand significantly greater hardware resources than a basic  $(15\text{-to-}1)$  configuration operating under the same code distances.

## C.3 Achieving utility with VQAs

Although near-term quantum platforms are inherently noisy, specific algorithmic frameworks—most notably variational quantum algorithms (VQAs)—offer a potential pathway to surpassing classical

computational capabilities. At its core, a VQA evaluates a parameterized quantum circuit (the ansatz) with respect to a problem-specific Hermitian operator (the Hamiltonian) to compute a scalar objective function, typically the system’s energy. This energy landscape is then navigated by classical optimization routines, such as Nelder-Mead or SPSA [95], which iteratively update the circuit parameters to locate the minimum. A key theoretical advantage of VQAs is their Optimal Parameter Resilience (OPR) [99], a property suggesting that the optimal parameter configurations discovered under noisy hardware conditions generally align with the ideal, noiseless solutions. In practice, however, the sheer magnitude of noise in the Noisy Intermediate-Scale Quantum (NISQ) era frequently overwhelms this inherent robustness, necessitating explicit error reduction techniques to solve complex, practical problems.

Historically, efforts to suppress errors on near-term hardware have heavily favored quantum error mitigation. Although a vast array of mitigation protocols has been developed for NISQ architectures [18, 77–79, 57, 46, 86, 28], these techniques alone have proven insufficient to bridge the gap to practical utility. To genuinely surpass classical computational capabilities, many VQA applications demand extremely high operational fidelities—often exceeding 99%—which mitigation alone struggles to deliver under severe hardware noise. Consequently, while advancing novel error mitigation strategies remains important, there is a growing consensus that transitioning toward early, lightweight, or partial implementations of quantum error correction is an unavoidable prerequisite for sufficiently suppressing noise and realizing true quantum advantage.

#### C.4 Solving combinatorial optimization problems with QAOA

Combinatorial optimization fundamentally involves identifying the optimal configuration from an exponentially large discrete search space. This paradigm underpins critical applications across logistics [85], finance [68], and operations research [76]. Because these problems are overwhelmingly NP-hard, finding exact classical solutions becomes computationally intractable as system sizes scale. In this context, problem formulation plays a pivotal role. The most common formulation is Quadratic Unconstrained Binary Optimization (QUBO), defined as  $\min x^T Q x$  where  $x \in \{0, 1\}^n$  and  $Q \in \mathbb{R}^{n \times n}$  is symmetric. This can be extended to Polynomial Unconstrained Binary Optimization (PUBO) to capture higher-order interactions ( $\min \sum_i a_i x_i + \sum_{i < j} b_{ij} x_i x_j + \sum_{i < j < k} c_{ijk} x_i x_j x_k + \dots$ ), and further generalized to Polynomial Constrained Binary Optimization (PCBO) by incorporating constraints. While PCBO models offer greater expressivity, they introduce significant computational complexity.

Classical exact solvers like CPLEX and Gurobi [43, 35] guarantee optimality through branch-and-bound and relaxation methods, but they suffer from exponential scaling. Conversely, heuristic approaches like simulated annealing and genetic algorithms [11] provide approximate scalability for larger problem instances. Often, PCBO structures are quadratized into standard QUBO forms [10, 2] to leverage existing solvers, though this comes at the expense of introducing auxiliary variables. Consequently, practically scaling these solutions continues to depend heavily on heuristic and approximation frameworks [52, 29].

To address these scaling limitations computationally, the Quantum Approximate Optimization Algorithm (QAOA) [22] offers a hybrid quantum-classical approach tailored for optimization tasks. A standard QAOA circuit is constructed by alternately applying  $p$  layers of two parameterized unitaries: a problem-specific cost operator  $U(\gamma, H_C) = e^{-iH_C \gamma}$  and a mixing operator  $U(\beta, H_M) = e^{-iH_M \beta}$ . Starting from an initial uniform superposition of all computational basis states,  $|s\rangle = \frac{1}{\sqrt{2^n}} \sum_z |z\rangle$ , the system is variationally evolved for  $p$  repetitions to approximate the low-energy configurations of the target cost Hamiltonian  $H_C$ .

Unlike the Variational Quantum Eigensolver (VQE), which typically targets physical ground states, QAOA is specifically designed to minimize classical discrete cost functions. However, because the standard QAOA ansatz restricts expressivity through its rigid, problem-specific layered structure, navigating its non-convex, instance-dependent optimization landscape is notoriously difficult [100, 23, 4, 39, 62, 16, 58, 19, 36, 93]. While increasing the circuit depth ( $p$ ) theoretically improves expressivity, it concurrently amplifies noise susceptibility on near-term hardware.

An alternative strategy to enhance expressivity without deepening the ansatz is to expand the classical parameter space per layer via multi-angle QAOA (ma-QAOA) [41]. Rather than tying all operations in a layer to a single pair of variables, ma-QAOA assigns independent variational angles to each

distinct term within the cost and mixer Hamiltonians:

$$U(H_C, \vec{\gamma}_\ell) = e^{-i \sum_{a=1}^m H_{C,a} \gamma_{\ell,a}} = \prod_{a=1}^m e^{-i H_{C,a} \gamma_{\ell,a}}, \quad (3)$$

$$U(H_M, \vec{\beta}_\ell) = e^{-i \sum_{b=1}^n H_{M,b} \beta_{\ell,b}} = \prod_{b=1}^n e^{-i H_{M,b} \beta_{\ell,b}}. \quad (4)$$

For a system with  $m$  clauses and  $n$  qubits, this expands the parameter count from the standard  $2p$  to  $(m+n)p$ . Standard QAOA naturally emerges as a special case of this formulation, whereas ma-QAOA allows classical optimizers to explore a vastly richer, multidimensional solution landscape.

Despite this increased expressivity, QAOA remains highly sensitive to parameter initialization [83, 8]. Poor starting configurations frequently trap the optimizer in suboptimal local minima or barren plateaus lacking useful gradient information [55]. Existing initialization heuristics, such as INTERP [104] or TQA [83], are typically customized for specific problem structures and struggle to generalize or scale seamlessly. This lack of robust, universally applicable initialization remains a major barrier to deploying QAOA for complex, real-world tasks.

Once a viable starting point is established, the continuous optimization loop updates the parameters within the interval  $[-\pi, \pi]$ —extending the search well beyond discrete Clifford angles. Depending on the landscape’s smoothness and the presence of hardware noise, this loop may employ gradient-free algorithms like COBYLA [103], SPSA [92], or Nelder-Mead [25], or gradient-based methods like L-BFGS-B [105] and Adam [50]. This iterative refinement proceeds until the algorithm converges or triggers a predefined iteration limit to conserve quantum resources.

Given the extreme non-convexity of the QAOA landscape, a single optimization trajectory—even one initialized with a high-quality warm-start—carries a substantial risk of converging to an unfavorable local minimum [83, 56]. To mitigate this vulnerability, multi-start optimization strategies [80] are widely employed, launching several independent optimization routines from a diverse collection of initial seeds to ensure robust convergence.

To empirically assess our work in the QAOA setting, we select a diverse set of optimization tasks. First, we leverage MaxCut as our primary QUBO benchmark. For a graph  $G$  with edge set  $E(G)$ , the corresponding cost Hamiltonian is defined as  $H_C = \sum_{(i,j) \in E(G)} \frac{1}{2} w_{ij} (I - Z_i Z_j)$ , where  $w_{ij}$  denotes the weight of edge  $(i, j)$ , and  $Z_i$  and  $Z_j$  are Pauli- $Z$  operators acting on the qubits associated with vertices  $i$  and  $j$ , respectively. MaxCut serves as an effective benchmark for evaluating our framework, enabling systematic analysis across varied graph topologies under a unified optimization setting. Specifically, we evaluate on weighted complete graphs, which exhibit dense connectivity, leading to highly entangled and globally coupled optimization landscapes.

For PCBO evaluation, we consider the Knapsack problem and a biomedical high-order interaction task [87] as representative benchmarks. The Knapsack problem is mapped to a PUBO Hamiltonian using the Qiskit Optimization module [75], where constraint satisfaction (e.g., capacity limits) is enforced through penalty terms. Problem instances are generated with randomized item weights and values to ensure a range of nontrivial optimization scenarios.

For the biomedical benchmark [87], each binary variable corresponds to a gene-associated feature, with bit assignments indicating selection within a subset. The PCBO representation captures both individual feature relevance and higher-order statistical dependencies—including pairwise and triple-wise mutual information—modeled as a weighted hypergraph. The objective is to select  $M$  features from a total of  $N$  candidates to maximize predictive relevance while reducing redundancy. This selection constraint is imposed via a Hamming-weight condition, enforced through an additional Lagrangian penalty term. In our experiments, we set  $M = 4$  for the MedicalDense tasks,  $M = 8$  for the 15-qubit MedicalSparse tasks, and  $M = 10$  for the MedicalSparse\_20 task. Further details regarding these QAOA benchmarks can be found in [6].

## C.5 Solving scientific problems with VQE

A prominent implementation of the VQA paradigm is the Variational Quantum Eigensolver (VQE) [95], which is explicitly designed to estimate the ground-state energy—or the minimum eigenvalue—of a target Hamiltonian  $\mathcal{H}$ . VQE has become a cornerstone algorithm in computational

physics and chemistry, routinely applied to compute molecular dissociation curves as a function of bond length or to resolve the minimum energy configurations of quantum spin models. Because of its practical importance, optimizing the reliable execution of VQE has been the subject of extensive architectural and systems-level research [78, 33, 98, 77]. In this study, we leverage VQE to investigate fundamental physical systems, detailing the specific target models below.

Within the realm of statistical mechanics, the Ising [17] and Heisenberg [9] models serve as foundational frameworks for describing interacting magnetic spin systems. These models are renowned for hosting rich quantum phenomena, including dimension-dependent phase transitions and highly entangled, non-classical ground states. Our analysis specifically targets one-dimensional configurations governed by uniform coupling parameters. The first is the one-dimensional transverse-field *Ising model*, defined by the Hamiltonian:

$$\mathcal{H} = J \sum_{i=1}^{N-1} X_i X_{i+1} + \sum_{i=1}^N Z_i. \quad (5)$$

This operator models a chain of  $N$  coupled spins (qubits) where nearest-neighbor interactions along the  $x$ -axis are governed by a coupling strength  $J$ , while each spin simultaneously interacts with a uniform external magnetic field of unit strength aligned along the  $z$ -axis.

Additionally, we examine a restricted variant of the field-free Heisenberg model, which generalizes spin-spin coupling across all spatial dimensions. Specifically, we focus on the Hamiltonian:

$$\mathcal{H} = \sum_{i=1}^{N-1} (JX_i X_{i+1} + JY_i Y_{i+1} + Z_i Z_{i+1}). \quad (6)$$

In this formulation, the system's energy scale is normalized by fixing the  $ZZ$ -interaction at unit strength. Because the transverse interactions along both the  $X$  and  $Y$  axes are constrained to share an identical coupling constant  $J$ , this specific parameterization is conventionally identified as the *XXZ model*.